Journal of Electroceramics 2:4, 229–242, 1998

Pyroelectric Sensors

M.H. LEE, R. GUO & A.S. BHALLA
Materials Research Laboratory, The Pennsylvania State University, University Park, PA 16802, USA

Submitted April 2, 1998; Revised April 2, 1998; Accepted July 28, 1998

Abstract. Status of the pyroelectric sensors is reviewed in brief. In this content the existing new materials, their pyroelectric properties, and figure of merit for various pyroelectric devices are compared. The assemblage components of a single pyroelectric sensor are reviewed and the discussions are extended to incorporate the large area and the multi-element devices suitable for wide range of applications.

Keywords: pyroelectric sensors, pyroelectricity, infrared sensors, ferroelectric materials and devices

1. Introduction

Pyroelectric sensors, in principle, work as a thermal transducer. The pyroelectric sensing element converts the non-quantified thermal flux into the output measurable quantity like charge, voltage or current. Therefore in designing and fabricating the sensor, the knowledge of the basic characteristics of the materials is desirable as those provide the understanding of several unforeseeable noise sources which occur from microphonic effects, clamping, mechanical strain, mounting of sensing elements, and packaging. This also provides the guidance in bonding of the sensing element and other thermal efficiency related problems. Thus there are two major considerations when fabricating pyroelectric sensors namely, (i) materials and (ii) design parameters.

In this article we discuss the sensor topic in the context of (i) characteristics of pyroelectric materials relevant to sensors and (ii) basic sensor design.

In the first part, the basics of the pyroelectric effect, evaluation of pyroelectric properties and material figures of merit for various pyroelectric devices are briefly discussed.

In the second part, comments are made on the status of different components of a pyroelectric sensor. The comments are extended to cover the various intrinsic and extrinsic noise factors that limit device performance and the design approaches to fabricate large and multi-element pyroelectric devices.

1.1. Pyroelectric Effect

The pyroelectric coefficient (p) of a material under constant stress and electric field is defined by the expression

$$p = \left(\frac{\partial P}{\partial T}\right)_{E,\sigma} \tag{1}$$

where P is the polarization, T the temperature, E the electric field, and σ the elastic stress [1–3].

The pyroelectric effect can be observed only in those materials whose point group symmetry is consistent with the vectorial property of the polarization. Thus crystalline materials whose structures belong to the ten polar point groups namely, *1, m, 2, mm2, 3, 3m, 4, 4mm, 6, 6mm* and ceramics, polymeric and composite materials whose structures belong to the textural or basic Curie point groups (∞,∞m) are pyroelectric materials. Thus the pyroelectrics can be classified into two main categories, (i) non-ferroelectric pyroelectrics, those whose polarization can not be switched by an application of external electric field (including some semiconductors and biological materials) and (ii) ferroelectric pyroelectrics those

whose polarization is obtained by poling and also can be switched by an electric field.

The pyroelectric effect of ferroelectric pyroelectrics usually exists below a certain transition temperature called the Curie point, T_c, in the proper ferroelectrics and is more temperature dependent than that of the non-ferroelectric pyroelectrics.

1.2. Primary and Secondary Pyroelectric Effects

Thermodynamic analysis of the pyroelectric effect yields the expression

$$p_i^\sigma = p_i^\varepsilon + d_{ijk}^T c_{jklm}^{T,E} \alpha_{lm}^\sigma \tag{2}$$

where p_i^σ is the total pyroelectric effect measured at constant stress, and p_i^ε, the pyroelectric effect at constant strain ε, is called the primary effect. The second term of Eq. (2) is the contribution caused by thermal deformation of the crystal and is known as the secondary pyroelectric effect. The d, c, and α are the piezoelectric, elastic stiffness, and the thermal expansion coefficients of the crystal, respectively. (A third contribution to the pyroelectric effect, known as the tertiary pyroelectric effect [4], arises from inhomogeneous temperature distributions within the sample. Since the origin of the tertiary effect depends on experimental conditions, it is not included in the present article.)

In ferroelectric pyroelectrics, the primary effect, in general, is large and negative because the spontaneous polarization diminishes with increasing temperature. The secondary effect is considerably smaller and may have either sign depending on the values of the constants. Thus the experimentally observed pyroelectric coefficients are dominated by the primary effect and are negative in ferroelectric crystals. In non-ferroelectric pyroelectric crystals there is no simple way to predict the sign and the magnitude of these coefficients. In practice the total pyroelectric effect can be measured and the secondary effect calculated from the constants d, α, and c.

For a number of applications, such as infrared detectors and vidicons, it is desirable to know the magnitude and sign of the contributions to the total pyroelectric effect. The secondary contributions for various crystal symmetry groups can be calculated from the following equations:

$$\begin{aligned} p_{\text{sec}} = {} & d_{21}(c_{11}\alpha_1 + c_{12}\alpha_2 + c_{13}\alpha_3 + c_{15}\alpha_5) \\ & + d_{22}(c_{12}\alpha_1 + c_{22}\alpha_2 + c_{23}\alpha_3 + c_{25}\alpha_5) \\ & + d_{23}(c_{13}\alpha_1 + c_{23}\alpha_2 + c_{33}\alpha_3 + c_{35}\alpha_5) \\ & + d_{25}(c_{15}\alpha_1 + c_{25}\alpha_2 + c_{35}\alpha_3 + c_{55}\alpha_5) \end{aligned} \tag{3}$$

for point group *2* and *b* as polar axis;

$$\begin{aligned} p_{sec} = {} & d_{31}(c_{11}\alpha_1 + c_{12}\alpha_2 + c_{13}\alpha_3) \\ & + d_{32}(c_{12}\alpha_1 + c_{22}\alpha_2 + c_{23}\alpha_3) \\ & + d_{33}(c_{13}\alpha_1 + c_{23}\alpha_2 + c_{33}\alpha_3) \end{aligned} \tag{4}$$

for point group *mm2* and *c* as polar axis; and

$$\begin{aligned} p_{sec} = {} & 2d_{31}(c_{11}\alpha_1 + c_{12}\alpha_1 + c_{13}\alpha_3) \\ & + d_{33}(2c_{13}\alpha_1 + c_{33}\alpha_3) \end{aligned} \tag{5}$$

for point groups *3, 3 m, 4, 4 mm, 6, 6 mm* and *c* as polar axis.

Point group ∞m of the poled ceramic sample leads to equations equivalent in form to the hexagonal crystal system. The ∞ axis is parallel to the poling direction and is denoted as x_3. A few materials with their primary and secondary pyroelectric components are listed in Table 1.

The values of the constants are taken from the literature and from the Landolt-Börnstein Tables on physical constants of materials [5]. It is evident from the data that in ferroelectric ceramics and single crystals, both the primary and total pyroelectric effects are large and negative. Secondary coefficients in ferroelectric single crystals are comparatively small and positive with the exception of $(Sr,Ba)Nb_2O_6$ (SBN) and $NaNO_2$ where the secondary pyroelectric effect is small and negative, enhancing the primary pyroelectric effect. In the case of triglycine sulfate (TGS), $Ba_2NaNb_5O_{15}$, and the ceramics lead zirconium titanate (PZT) and $BaTiO_3$, the secondary effect is substantial.

Compared to ferroelectrics, tourmaline and other non-ferroelectric polar materials show rather small pyroelectric effects. In these materials, the total and the secondary coefficients carry the same sign, and in most cases they are positive. The secondary effect, arising from piezoelectricity and thermal expansion makes a large contribution to the total pyroelectric effect. In tourmaline for instance, 80% of the pyroelectric effect is of secondary origin. Fresnoite, $Ba_2TiSi_2O_8$, is another mineral in which pyroelectricity is dominated by the secondary effect. In semiconductor pyroelectrics with the wurtzite

Table 1. Primary, secondary, and the observed pyroelectric effects in various pyroelectric materials (Room temperature values)

Materials	Point group symmetry	Observed total effect $\mu C/(m^2-K)$	Calculated secondary effect $\mu C/(m^2-K)$	Primary effect $\mu C/(m^2-K)$
A) Ferroelectrics				
a) ceramics				
$Pb(Zr_{0.52}Ti_{0.48})O_3$:1 wt%$Nb_2O_5$ (PZT)	∞m	−50	+60	−110.0
$BaTiO_3$	∞m	−190.0	+80.0	−270.0
$Pb(Zr_{0.95}Ti_{0.05})O_3$:1 wt%$Nb_2O_5$(PZT)	∞m	−268.0	+37.7	−305.7
b) single crystal				
$Sr_{0.5}Ba_{0.5}Nb_2O_6$(SBN)	4 mm	−550	−21.0	−529.0
$(NH_2CH_2COOH)_3 \cdot H_2SO_4$ (TGS)*	2	−270	+60.0	−330.0
$LiTaO_3$	3 m	−176	+2.00	−178
$LiNbO_3$	3 m	−83.0	+12.9	−95.9
$Pb_5Ge_3O_{11}$	$\bar{3}$	−95.0	+15.5	−110.5
$Ba_2NaNb_5O_{15}$**	2 mm	−100.0	+41.8	−141.8
$NaNO_2$	2 mm	−140.0	−5.0	−135.0
B) Non-ferroelectrics				
$Li_2SO_4(H_2O$	2	+86.3	+26.1	+60.2
tourmaline	3 m	+4.0	+3.2	+0.8
bone	∞	$+25\times10^{-4}$	$+117\times10^{-4}$	-92.0×10^{-4}
$Ba_2Si_2TiO_8$ (Fresnoite)	4 mm	+10	+22, +16	−12.0, −6.0
Li_2GeO_3	2 mm	−27	−12.8	−14.2
$Ba(NO_2)_2(H_2O$		−25.3	−3.3	−22.0
C) Semiconductors (Wurtzite structure)				
CdS	6 mm	−4.0	−1.0	−3.0
CdSe	6 mm	−3.5	−0.56	−2.94
ZnO	6 mm	−9.4	−2.5	−6.9
ZnS***	6 mm	0.43	+0.34	
BeO	6 mm	−3.40	−0.008	−3.39

*) Average value of the wide range of reported values between 200 to 350 $\mu C/(m^2-K)$.
**) Maximum value of p measured on the sample.
***) No reported sign for p^σ; no information about polytypic nature of the sample.

structure, the effect is very small, with all coefficients having the same sign.

It is clear from the Table 1 that both the primary and secondary effects are important, and the certain trends emerge regarding the magnitude and sign of the coefficients. All pyroelectric materials do not follow the same pattern, but members of the same family share common features: In ferroelectrics all the observed coefficients are negative and dominated by the primary effect, in contrast to non-ferroelectric pyroelectrics where secondary effects could be more substantial.

1.3. Methods for Determination of Pyroelectric Coefficients

There are several methods for measurements of pyroelectric coefficients but most of those can be grouped into two categories [2,3]. The objective in the first case is to directly measure the pyroelectric current and at the same time vary the temperature. In the second approach measurements of polarization or charge can be estimated either by the integration of pyroelectric current during the continuous heating of the sample or recording the hysteresis loop at various temperatures by the Sawyer-Tower technique.

In the first approach the varying temperature can be generated by using the chopping incoming radiation source or ac heating (known as Chynoweth technique) of the sample and the pyroelectric response current i can be expressed as [2,6]:

$$i = \frac{p\eta W T_r}{Ct} \tag{6}$$

where ηW is the power absorbed by the sample, T_r is a

transfer function depending on the thermal circuit of the sample and the chopping or modulation frequency, t is the thickness of the sample, C' is the thermal capacity of the sample. Often a thin layer of highly absorbing material is applied on the sample surfaces in order to achieve $\eta = 1$.

The pyroelectric current $i(T)$ at a temperature T, can also be measured by uniformly heating or cooling the sample at a constant rate (in general 1 to 4°C/min) and the pyroelectric coefficient, p, can be calculated by using the following expression (Byer-Roundy technique) [7]:

$$i(T) = \frac{Ap}{(\Delta T/\Delta t)^{-1}} \tag{7}$$

where A is the electroded area of the sample, $\Delta T/\Delta t$ is the heating or cooling rate of the sample.

In the second approach the charge release (in either of the two cases mentioned earlier) at a discrete temperature is determined and the pyroelectric coefficient is obtained by graphically or by differentiation.

1.4. Pyroelectric Material Figure of Merit

Pyroelectric materials have found application in a wide range of fields.

For device applications and the convenience of application engineers, several figures of merit criteria are defined. Most of these can be calculated using the thermal, electrical and optical characteristics of the materials available in the literature and various handbooks on the physical constants of materials [5]. The four major figures of merit are listed below:

(i) $F_D = \dfrac{p}{C_p \rho \sqrt{\varepsilon_0 \kappa \tan \delta}}$ pyroelectric point detector

(ii) $F_i = \dfrac{p}{C_p \rho}$ fast pulse detector

(iii) $F_v = \dfrac{p}{C_p \rho \varepsilon_0 \kappa}$ large area detector

(iv) $F_{\text{Vid}} = \dfrac{p\gamma}{C_p \rho \varepsilon_0 \kappa}$ vidicon

where C_p is the specific heat, ρ is the density, ε_0 is the vacuum permittivity (8.85×10^{-12} F/m), κ is the dielectric constant, tan δ is the dielectric loss tangent, γ is the reciprocal thermal diffusivity and p is the pyroelectric coefficient of the material at the operating temperature of the device [8].

While expression (i) evaluates the material characteristics for the point detector, the figure of merit (ii) is sufficient to select suitable materials for fast high power laser pulse detectors. Expression (iii) is good for large area detectors. For an infrared imaging systems, where array designs are desirable, expression (iv), which includes the thermal diffusivity aspects, is the suitable one.

1.5. Induced Pyroelectric Effect

In several pyroelectric device designs an induced pyroelectric effect (under an applied electric field) has been exploited. The induced pyroelectric coefficient, p_{ind} is defined as:

$$p_{\text{ind}} = \varepsilon_0 E \frac{d\kappa}{dT} \tag{8}$$

where E is the applied field and T is the temperature. The sign of the p_{ind} is defined by the electric field vector. The material figure of merit for this category is expressed as

$$\frac{p_{\text{ind}}\gamma}{C_p \rho \sqrt{\kappa(E) \tan \delta(E)}} \tag{9}$$

where $\kappa(E)$ and $\tan\delta(E)$ are the dielectric constant and the dielectric loss factor respectively, of a material at a specific electric field.

Materials of interest in this category are usually high dielectric constant relaxor ferroelectric ceramics and crystals with dispersive nature and Curie point near room temperature. These materials are important for large area infrared imagers.

It is clear from the above expressions that high p/κ is the first clue for the selection of a suitable material for pyroelectric devices.

1.6. Important Candidate Materials

The most suitable candidate materials for pyroelectric devices are listed in Tables 2 and 3 [8,9].

Several modified TGS compositions have attractive pyroelectric properties (Table 3) and are thus useful for the highly sensitive IR imagers. In Table 3, the various letters represent D = deuterium, B = beryllium, F = fluorine, M = manganese, P = phosphorous, As = arsenic, L = lithium, and

Table 2. Pyroelectric Properties of Important Pyroelectrics at 25°C

Material	p (μC/m^2 K)	Dielectric properties κ	tan δ	C_P (10^6 Jm^{-3} K^{-1})	K (10^{-7} m^2 S^{-1})	T_c (°C)	F_V (m^2 C^{-1})	F_D (10^{-5} Pa$^{-1/2}$)	F_{vid} (10^6 sC^{-1})
PVDF	270	12 (10 Hz)	0.015 (10 Hz)	2.43	0.62	80+	0.1	0.88	1.6
LiTaO3	230	47	10^{-4} to 5×10^{-3}	3.2	13.0	665	0.17	35.2 to 4.9	0.13
[1]SBN50	550	400	3×10^{-3}	2.34		121	0.07	7.2	
[2]PZFNTU Ceramics	380	290 (1 kHz)	2.7×10^{-3} (1 kHz)	2.5		230	0.06	5.8	
[3]PCWT 4/24 Ceramics	380	220 (1.5 kHz)	0.011 (1.5 kHz)	2.5		255	0.08	3.3	
[4]PGO	110	40	5×10^{-4} (100 Hz)	2.0	3.0	178	0.16	13.1	0.5
[5]PGO:Ba3	320	81	1×10^{-3} (100 Hz)	2.0	3.0	70	0.22	8.4	0.7
TGS	550 (35°C)	55	0.025	2.6	3.3	49	0.43	6.1	1.3
DTGS	550 (40°C)	43	0.020	2.4	3.3	61	0.60	8.3	1.8
TGFB	700 (60°C)	50	0.028	2.6	3.3+	73	0.61	7.6	1.8
ATGSAs	700	32	<0.010			51	0.99*	>16.6*	3.0

[1] SBN50—$Sr_{0.5}Ba_{0.5}Nb_2O_6$.
[2] PZFNTU—$PbZrO_3$:$PbTiO_3$:$PbFe_{0.5}Nb_{0.5}O_3$.
[3] PCWT4/24—$(Pb_{0.76}Ca_{0.24})(Co_{0.5}W_{0.5})_{0.04}Ti_{0.96}O_3$.
[4] PGO—$Pb_5Ge_3O_{11}$.
[5] PGO—Ba3: $Pb_{4.7}Ba_{0.3}Ge_3O_{11}$.

Table 3. Pyroelectric properties of the TGS family (optimum temperature)

Material	κ	p (μC/m^2 – K)	P_s (μC/cm^2)	T_c (°C)	p/κ (10 μC/m^2 – K)
TGS	30	330	3.0	49	1.1
DTGS	19	270		62	1.4
TGFB	14–16	210–140		73	1.5
DTGFB	11–14	190–240	4.3	75	1.7
LTGS	40	400	3.7	49	1.0
MTGS	40	560	4.6	49	1.2
ATGSP (25°C)	30–32	650	5.0	51	2.0
ATGSAs (25°C)	32	700	6.0	51	2.1–2.3
ADTGSP	22	460	5.3	60	2.1
ADTGSAs	23	500	6.2	62	2.2

A = alanine, and these elements have been used for the doping or modification of TGS.

Figure 1 shows typical values of p, κ, and p/κ and their temperature dependencies for the single crystal of ATGSAs.

In proper ferroelectrics, a simple phenomenological approach is suggested to relate the pyroelectric figure of merit p/κ to more basic parameters of the pyroelectric crystals [10,11]. For a very wide family of displacive and order-disorder ferroelectrics, an empirical relation $p/\sqrt{\kappa} = 3 \times 10^{-9}$ C · cm^{-2} · deg.$^{-1}$ applies where as for several modified triglycine sulfate (TGS) crystals the relation $p/\kappa^{3/4} = 3 \times 10^{-9}$ C · cm^{-2} · deg.$^{-1}$ holds nicely. Figure 2 summarizes the results for most ferroelectric pyroelectrics.

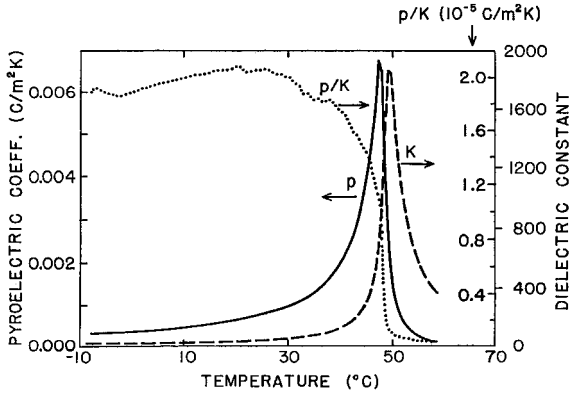

Fig. 1. Temperature dependence of p, κ, and p/κ for ATGSAs (alanine and arsenic doped triglycine sulphate) crystal.

2. Pyroelectric Devices

The pyroelectric device is a thermal sensor, wherein the light power is converted to an electrical output. Its response is independent of the wavelength of light or radiant energy it receives. The pyroelectric detector is especially useful for the near to far infrared (IR) because of its high sensitivity and the good transmittance of IR in air (when using a proper window material).

2.1. Sensor Assemblage

Figure 3 gives a typical design of pyroelectric single element detector, which consists of a window, a sensing element, and integral electronics (readout integral circuit).

2.1.1. Window. The window restricts incoming light to a wavelength band of interest, and it protects the sensing element and internal electrical circuits from physical and/or chemical damage and moisture. The properly selected window can have a function of an optical filter that blocks unwanted wavelengths and passes desired wavelengths.

The type of window as filter could be chosen [2] with the consideration of applications and to eliminate the possible interfering radiation. In general, four kinds of filters are used as the window, such as low-pass, high-pass, narrow-band, and wide-band filters. The single crystals of Ge, Si, Al_2O_3, and ZnS, which are coated with many layers of MgF_2, BaF_2, PbF_2, CaF_2, and ZnSe, are used as the filter for the IR region [12–16].

Following the theory of blackbody radiation, the intensity of a radiated wave shows a wavelength

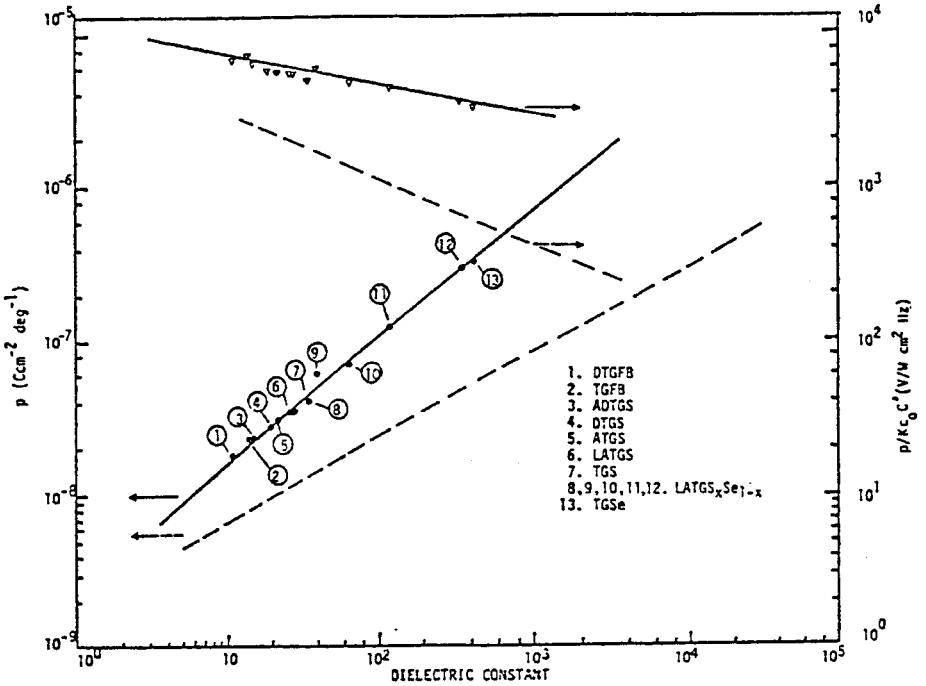

Fig. 2. Pyroelectric coefficients and pyroelectric figure of merit $p/\varepsilon_0\kappa C$ vs. dielectric constant, for various proper ferroelectric materials. Solid lines and broken lines represent the TGS family and the displacive & order-disorder ferroelectrics respectively ($C = \rho C_P$).

distribution at the object temperature. The wavelength of maximum intensity will be the most practical guide for objects. The Wien's law can give the wavelength (λ) of the maximum intensity in micrometers; $\lambda = 2{,}893/T$, where T is in Kelvin [K] [17]. In case of detecting the presence of a person, the intensity near 10 μm in wavelength shows the peak value. Possible sources of interference are the reflected and head lights in the visible range. Since the wavelength of maximum intensity for interferences are shorter than 10μm, a window of long-pass or low-pass filter type is required. For detection of molecular gases, a narrowband or very restrictive bandpass window might be required.

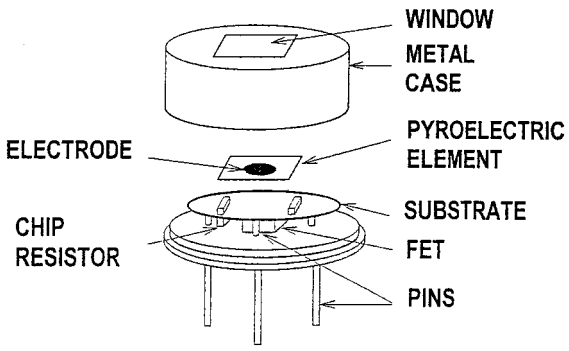

Fig. 3. Typical design of a single element pyroelectric detector.

2.1.2. Sensing element. The sensing element of a pyroelectric detector is a thin wafer of single crystal or ceramic. The material has a high Curie point (T_c), high figures of merit F_V, F_I, F_D, and good thermal and mechanical properties. The layout, electrode design, and packaging for the sensing element will be discussed in the later sections.

2.1.3. Integral electronics. When the detector is heated by incident radiation, the temperature change might result in polarization changes, which appear as charge on the capacitor formed by the pyroelectric with its two electrodes. Since this capacitance is fairly small, the detector itself has very high ac impedance. In most applications, these very high ac and dc impedances must be converted to a more practical low impedance output. In order to detect this small charge, low-noise and high-impedance amplifiers are necessary [13,17].

This can be done in two ways [13,17,18]: a voltage follower and a current amplifier. The voltage mode circuit (a voltage follower) will yield the best signal-to-noise (S/N) ratio and low output impedance. It can operate at a very small supply voltage and current, i.e. low power consumption. However, it does not have a large output responsivity, which varies with frequency. The current mode offers substantial increase in output signal—high responsivity, which is independent of frequency. Unfortunately, the noise characteristics of the amplifier limit the S/N ratio that it requires the high operating voltage and current. Though the voltage or current mode circuit can be used as readout circuit, the additional stray-capacitance, RF pickup, compromise in reliability, testing problem, and the cost will be the major concerns. To overcome these problems, a simple FET (JFET or MOSFET) with an appropriate load resistor or OP-AMP with feedback resistor in the detector package is suggested as the most common arrangement. The resistance of a load or feedback resistor is in the range of gigaohms. These high quality bias resistors must have good environmental stability, low temperature coefficient of resistance (TCR), and low voltage coefficient of resistance (VCR). Since the output of the pyroelectric sensor is proportional to the product of the pyroelectric current and the bias resistance, TCR and VCR result in the nonlinearity of the overall transfer function of the sensor.

2.2. *Performance of the Detector*

2.2.1. Pyroelectric response. In order to analyze the performance of pyroelectric detectors, both the thermal and electrical equivalent circuits should be considered [18,8]. Figure 4 shows a typical arrangement of practical detectors. When a pyroelectric detector is exposed to radiation power $W(t) = W_o e^{i\omega t}$, modulated at a frequency ω, the temperature of the sensing element of the detector would also be modulated at ω by an amount which depends on the light absorptance η, heat capacitance H_T, and thermal conductance G_T. The temperature difference (θ) between the sensing element and its surroundings is described by Eq. (10):

$$\eta W(t) = H_T(d\theta/dt) + \theta G_T \tag{10}$$

which has the solution,

$$\theta = [\eta W_o e^{i\omega t}]/[G_T + i\omega H_T] \tag{11}$$

where t is time. The current responsivity (R_I) is defined as,

$$R_I = I/W_o = (dq/dt)/W_o = [d(pA\theta)/dt]/W_o = (\eta pA\omega)/[G_T(1 + \omega^2\tau_T^2)^{1/2}] \tag{12}$$

where I, q, A, p, τ_T represent the current, pyroelectric charge, electrode area of detector, pyroelectric coefficient, and thermal time-constant ($=H_T/G_T$), respectively. The voltage responsivity (R_V) is defined as:

$$R_V = V/W_o = [I/(G_E + i\omega C_E)]/W_o = (\eta pA\omega)/[G_T G_E(1 + \omega^2\tau_T^2)^{1/2}(1 + \omega^2\tau_E^2)^{1/2}] \tag{13}$$

where G_E, C_E, $_E$ are the electrical conductance, capacitance, and time constant ($=C_E/G_E$), respectively. With Eq. (12) and (13), references 19 and 20 propose a procedure for the analysis of thermal properties by use of step-signal radiation. Following Eq. (12) and (13), small G_T and large values of η, p, and A of the detector are required for obtaining the high outputs.

Good thermal isolation of the thin pyroelectric sensing element from the surroundings result in a small G_T. Several methods for thermal isolation, especially by support of the thin sensing element, have been suggested. The use of a conducting spherical ball is one method, but this cannot offer simple fabrication and stable performance of the detector. The detector consists of a thin circular crystal plate coated with circular surface electrodes and is mounted on a shallow cylindrical substrate. Oettel [21] proposed a pyroelectric detector mounted on several arch-like metal wires attached to the base or mounting platform. The sensing element can be raised above the base by means of springs

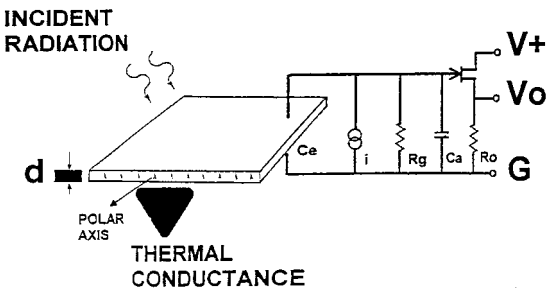

Fig. 4. Equivalent circuit of a pyroelectric detector.

(Matsushita) and wires (Eltec) [13]. It can also be mounted on adhesive posts, bars, hollow base (Murata), and mica plates of low thermal conductivity. In addition, a PEC (pyroelectric materials on an electric conductor) structure with air-gap was proposed by Kuwano et al. [22]. In case of staring array, a sensing element supported on a silicon substrate by microbridges (GEC-Marconi) had been fabricated by anisotropic etching [23,24].

The light absorptance (η) of electrode sensing elements can affect the output of the detector. In order to increase η, a metallic thin film, metal-black paste, and evaporated or electroplated metal-black are commonly used as the light absorbers [25,26]. Recently, in the case of array-type devices, multilayer absorbers with single cavities (SCA) [27] and with double cavities (DCBA) [28] were proposed for use as the light absorber.

The performance of pyroelectric detectors has been enhanced through the improvement of pyroelectric materials, fabrication techniques, sensor layout, and sensor systems. In general, the incident IR is periodically chopped for the ordinary pyroelectric detector in order to generate a continuous output voltage or current. However, the chopping system is large in size, requires high power, and shows low reliability. Shibata et al. [29–31] proposed the modulation type pyroelectric detector (M-type IR detector) which is composed of a sensing part and a solid-state chopper with two piezoelectric bimorph-vibrators and two slit-plates in the same package. This features high reliability, small volume, and low power consumption compared with conventional detectors using a rotating chopper.

2.2.2. Noise factors. The response and noise of a detector must be considered when analyzing its usefulness for a particular application. The usefulness of a detector can be expressed in many different ways [8,18,32]. One of the most useful and practical consideration is the noise-equivalent power (NEP). This is defined as the incident power that is required to produce a signal to the rms noise voltage (V_N):

$$\mathrm{NEP} = V_N/R_V \tag{14}$$

Occasionally, if the detector is placed into a uniform radiation field, the noise-equivalent irradiance (NEI) is a more relevant performance figure of merit, and is defined as:

$$\mathrm{NEI} = \mathrm{NEP}/A \tag{15}$$

This enables one to compare the ability of different sized devices to detect a given irradiance or incident power density. The NEP is usually expressed in units of $\mathrm{WHz}^{-1/2}$ (being specified for a particular frequency and unit bandwidth), or in W (being the ratio of broadband noise to responsivity at a specified frequency). Similarly, the NEI is expressed in $\mathrm{Wm}^{-2}\mathrm{Hz}^{-1/2}$ or Wm^{-2}. Furthermore, the reciprocal of NEP is defined as the detectivity (D); and the specific detectivity (D^*) is defined as :

$$D^* = A^{1/2}/\mathrm{NEP} \tag{16}$$

that is normalized to unit bandwidth. The D^* is expressed in $\mathrm{mHz}^{1/2}\,\mathrm{W}^{-1}$. If the noise source is proportional to $\mathrm{A}^{1/2}$, D^* is independent of area and can be used to compare the merits of detectors with different size electrodes. However, this condition is not always satisfied and D^* must be used with caution.

There are three major noise sources in a simple pyroelectric detector : thermal noise (V_t), dielectric noise (V_d: Johnson noise), and amplifier noise (V_e : input-voltage noise, V_i : input-current noise, V_r : shunt-resistor noise), which are expressed as Eq. (17–21):

$$V_t = R_V(4kT^2G_T)^{1/2}/\eta \tag{17}$$

$$V_d = (4kT\omega R^2 C_E \tan\delta)/(1+\omega^2{\tau_E}^2) \tag{18}$$

$$V_e = e_A[(1+\omega^2R^2{C_E}^2)/(1+\omega^2{\tau_E}^2)]^{1/2} \tag{19}$$

$$V_i = i_A R/(1+\omega^2{\tau_E}^2)^{1/2} \tag{20}$$

$$V_r = [4kTR/(1+\omega^2{\tau_E}^2)]^{1/2} \tag{21}$$

The total mean square noise voltage (V_N) may then be written as,

$$V_N^2 = V_t^2 + V_d^2 + V_e^2 + V_i^2 + V_r^2 \tag{22}$$

An indication of the relative magnitudes of these various sources of noise for a typical detector is given in Fig. 5. It has been assumed that both the thermal and electrical time constants are longer than one second. The loss-controlled Johnson noise dominates above about 20 Hz, while the thermal noise is insignificant and is often ignored in calculations.

Pyroelectric detectors could give unwanted outputs due to the environmental effects, such as temperature fluctuation (thermal cycling, rapid changes in ambient temperature), mechanical vibration, electromagnetic interference, and sudden relief of stress caused by the differences in the thermal expansion of packaging

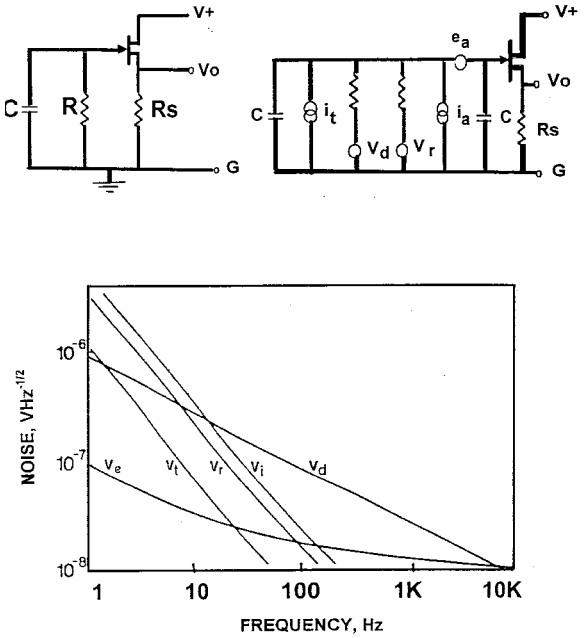

Fig. 5. (a) Noise sources and (b) relative magnitudes of noise voltages in a typical pyroelectric detector.

components [8,18,32,33,34]. These can give rise to microphonic (vibrational or acoustic) noise [35], thermally induced noise (transients), spurious noise pulses or spurious output signals [36–40]. Many methods have been proposed to eliminate the unwanted output signals, such as the use of less rigid mounting of pyroelectrics, single point supports, polycrystalline materials, electrically conducting windows, and good package design [17].

2.2.3. Compensated detectors. Mechanical clamping, as mentioned previously, can attenuate noise due to the ambient temperature changes and vibrational pickup. Further reductions in these sources of noise [8,18] have been achieved by using compensated detectors, as shown in Fig. 6 [13].

Byer et al. [41] fabricated pyroelectric detectors with a novel complementary domain configuration that reduced the interference from vibrational noise sources and from changes in ambient temperature by over an order of magnitude relative to the performance of conventional pyroelectric detectors. Compensation is obtained by connecting two oppositely polarized detector elements either in series or in parallel, the two elements must be of equal area if

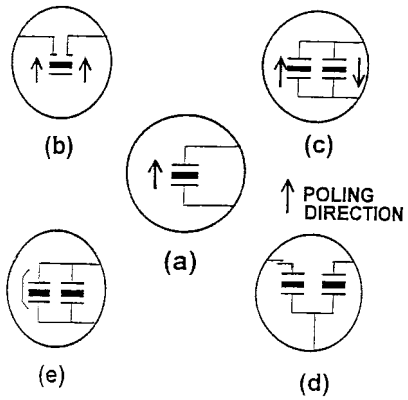

Fig. 6. Available configurations of pyroelectric sensing elements: (a) single element, (b) double-series element, (c) double-parallel element, (d) twin element, and (e) thermally compensated, shielded double element.

connected in parallel [17], with only one-element exposed to the IR radiation. Since environmental changes affect both elements alike, the signals from the two elements cancel each other, and no output is observed. Greater efficiency can be obtained where a moving target is viewed by arranging the system so that the image moves from one element to the other.

The double-serial (DS) detector is not much different from the single one apart from the changed frequency characteristics of noise and voltage response. Putley [42] calculated the performance of this type of detector. Following his calculation, the compensation would degrade R_V and NEP by a factor between $2^{1/2}$ and 2, depending on the frequency range and the dominant noise mechanism. It is easy to form the functional patterns on the sensing element. A modified circuit [43], in which one channel is unbalanced by an additional capacitor, has been proposed to improve the frequency-dependent CMRR (common-mode rejection ratio), where CMRR at low frequency is higher than that at high frequency, and the turbulence signals are shifted to higher frequency. This circuit is useful for motion detectors because of its improved CMRR property with frequency [44].

The double-parallel (DP) detector is difficult to construct due to connections between the electrodes. The usual solution is to mount the two separate thin crystalline sensing elements on the separate holders. However, this technique lacks uniformity and precise cancellation of common mode. Lavrencic et al. [45] have suggested one method to construct a DP detector

with two-antiparallel elements on the same sensing wafer, which provides almost identical sensing material with resulting compensation of common modes. The design offers excellent microphonics rejection.

3. Dielectric Bolometers

All the pyroelectric detectors discussed above are based on the ferroelectrics operated below T_c, where the material has a finite built in polarization. However, it is possible to operate the ferroelectrics under an applied dc bias field at or above T_c, the so-called dielectric bolometer mode [8,12,32]. The induced pyroelectric coefficient (p') is then expressed as:

$$p' = (dD/dT)_E = (dP_S/dT)_E + E(d\kappa/dT)_E \tag{23}$$

The coefficient p' can be inserted in the standard figure of merit (or responsivity) discussed above, together with the appropriate dielectric constants and losses measured at the relevant field and temperature.

Of particular interest with this mode of operation is the fact that much lower losses can be observed because of freezing in domain wall motion by high dc bias. Furthermore, the losses also have a tendency to reduce with increasing bias field. It is expected that dielectric bolometers may offer marked improvements in the detectivity (D, D^*) relative to the more conventional pyroelectrics. The reduced losses by dc bias field had been observed in the ferroelectric state, especially at the transition temperature much lower than T_c. However, the method of dc biasing the sensing element is not easy and the dc power supply is very expensive for the application of a single- or dual-element device.

For commercial purposes, GEC-Marconi [23] has built up the staring array for the thermal imaging camera by using $Pb(Sc,Ta)O_3$ thin films, and Texas Instrument [46] has also manufactured the thermal imaging targets of 2-D arrays for the IR camera by use of $(Ba,Sr)TiO_3$ ceramic wafers prepared by hot-pressing. In order to obtain good thermal isolation of sensing element to their surroundings, especially to IC Si wafers for readout, both companies have manufactured the sensors as hybrid-types by using the solder-bump technique.

4. Single and Multi-element Devices

Various factors including the pyroelectric material used, the dimensions of the sensing element, the electrode structure, the method of mounting the element, the value and type of the bias resistor, and the type of FET used can affect the detector performance [8,17,18]. Only a few published reports on the technology of pyroelectric detectors, deal mainly with the problems of single detectors. The main difficulties involve the thinning of the crystal wafers, electroding, detector structure (layout), and assembling the various parts (FET, gigaohm(s) resistor, support structures, detector can), together using epoxy glues and/or wire-bonds, thermally and mechanically insulating the sensing element from the supporting structure, developing the proper test procedure in order to assure the integrity and quality of design. The design should be optimized to accommodate mass production.

4.1. Single Element Detectors

A single element detector is housed in a metal TO-5, TO-8, or TO-39 can for better shielding and is protected from the environment by Ge or other appropriate window. Sometimes, the inner space of the can is filled with dried air or nitrogen [13,17].

Consideration can be given to both responsivity and noise. At low frequencies, the responsivity (R_V) decreases with decreasing chopping-frequency (ω) due to the electrical and thermal time constants of the circuit of detector. From Eq. (13);

$$R_V = (\eta p A \omega)/G_E G_T \tag{24}$$

in order to obtain high R_V, small values of G_E and G_T are required. In that case the bias resistor must be as large as possible and the detector should be well insulated from its enclosure.

The major source of noise depends on many factors [8,18], as shown in Fig. 5, with the FET current noise and bias-resistor noise being dominant. As mentioned above, two sensing elements are usually oppositely, in series or in parallel, connected for better compensation of rapid thermal changes and mechanical stresses resulting from acoustical noise and vibrations. Sometimes, one of the elements is coated with a light absorber, while the other element is shielded from radiation. Since most pyroelectrics are also piezoelectrics, they are susceptible to microphonics.

For better noise rejection, the sensing element must be mechanically decoupled from the outside, especially from the connecting pins and the metal can [17].

The structures of signal electrode and light absorber are also important in single-element sensors, because the responsivities R_V and R_I are dependent upon light absorptance (η) and thermal properties (H_T, G_T), where the thermal properties are dependent upon the electrode structure [19,20]. Many kinds of light absorber have been proposed [25,26], and the metal-blacks, especially gold-black, and the thin metallic films of NiCr, Ti, and Al are commonly used as a light-absorbing electrode because of their good thermal absorptance and small thermal mass characteristics. In order to obtain good electrical and thermal contacts between metallic electrodes and sensing wafer, thin films of Ti and NiCr are used as signal electrodes [19].

In many cases, good performance can be obtained through the use of thin sensing elements. This offers a reduction in dielectric, resistor, and current noise without affecting the responsivity. Considerable efforts have been devoted to making very thin sensing elements. One of them obviously is the thin film sensor approach [47]. Pyroelectric thin films on the Si readout IC have been prepared by various methods such as e-beam evaporation, sputtering, laser ablation, spin coating, and so on. Okuyama et al. [48] proposed the IR-OPFET (infrared-optical FET) type sensor with good performance. Several authors suggested the micromachined membrane structures [49] and IR-CCD sensors [50] prepared by deposition of ferroelectric thin films onto a Si-CCD.

4.2. *Multi-element Arrays*

For application of thermal imaging and laser beam profile monitoring, it is advantageous to use a detector consisting of an array of small elements: a linear and two-dimensional staring arrays. It is possible to use photoconductive or photovoltaic detectors of III-V or II-VI semiconductors, such as GaAs, and MCT ($Hg_xCd_{1-x}Te$) [51–53]. However, there are considerable technical problems for the use of these materials. They are difficult to grow and they require cooling, usually to 77 K or below for maximum efficiency of operation. It is true that excellent performance has been obtained with such materials, but the devices are very expensive, power-consumptive, and operate in a narrow radiation band.

Thermal images can be detected by thermally sensitive devices such as thermopiles, bolometers, and pyroelectric detectors, which offer very low cost, high performance, and low operational cost because of no requirement for cooling. The performances of the pyroelectrics are much better than those of thermopiles and bolometers. Recently, however, through the rapid improvement of manufacturing technologies, microbolometers match the pyroelectrics performance. On the other hand, the pyroelectric arrays need chopped thermal signals to obtain continuous thermal-images, but microbolometers do not require a chopper. Therefore, the pyroelectrics and the microbolometers are in close competition in the field of the development of two-dimensional uncooled arrays for thermal imaging [54].

Many reviews on the manufacturing technologies, design, performance, noise, systems, and applications for pyroelectric multi-element arrays are found in the existing literature [12,32,55–58]. Therefore, details of these are not repeated in this article, but there are some new developments that emerged recently and are worthy of comment. GEC-Marconi [59] has developed an uncooled pyroelectric IR camera with a 256×512 staring array, which has adopted microscan-chopping and video-support (625/50 Euroscope) up to 256 equivalent frames. This shows a $16\times$ improvement in S/N ratio, dynamic adjustment, wide dynamic range (200 K), excellent accuracy (0.1 K) and < 0.1 K of NETD (noise-equivalent temperature difference). Texas Instrument [60] has developed uncooled LWIR thermal sensors and systems, i.e. the LOCUSP weapon sight which shows $3\times$ magnification and 320×240 staring array of $(Ba,Sr)TiO_3$ ceramics. Measured sensitivity of less than 0.1 K of NETD is attractive for many military and commercial applications.

4.3. *Fabrication*

Scientists working in the sensor field are aware of rapid developments in new types of sensors over the past few years. In spite of the growth in the number of new IR sensor designs, there is still a large gap between a laboratory-created sensor chip and the realization of an industrially manufactured device [61]. Apparently, one of the reasons for this is the lack of development of fabrication technology and microstructural problems.

The general technological conception of a sensor

should be based on batch processing: i.e., the individual elements and the construction of the whole. It turns out that the most challenging problems are [62]: the joint between the sensor chip and package; output leads or cables and their connections to chips; protection elements against environmental effects; the micropackage itself and its assembly and the mounting elements. Providing environmental protection and individual sensor tuning must be carefully considered. Suggestions for solving such problems have already been made in earlier sections.

The most obvious advantages of sensors over conventional transducers are their small size and mass. Therefore, the problems of sensor and sensor package miniaturization become quite evident. Several ways of solving these problems are proposed, such as M-type detector (see in section 2.1), integrating the sensor with the readout electronics, and so on. In view of the sensor structure, two types of integrated sensors are suggested: hybrid and monolithic structures. The hybrid-type sensor can offer an excellent performance—very high sensitivity, good thermal isolation, and excellent NETD. However, it has a problem of higher manufacturing cost than the monolithic-type. Monolithic-type thermal sensors [24] are always very attractive, because they provide the advantage of on-chip sensor-processor integration, avoiding a laborious hybridization procedure as well as reducing electromagnetic interference noise. However, judging from the final objective of low-cost mass production of these sensors, one has to consider carefully the compatibility requirements for the VLSI technology.

5. Applications and Concluding Remarks

Pyroelectric sensors are capable of detecting IR sources and their size, temperature, direction of motion and speed, emissivity, and wavelength. Because of these characteristics, pyroelectric sensors have found many applications as single element detectors or in multi-element array structures [8,12,17,18,55–58]. As single element sensors, they are used as intruder alarms, fire alarms, pollution monitoring, chemical (gas) analysis [29,30], spectroscopy (radiometer) [63], laser detectors and energy meters [64], thermal recording [65], microphones [66], calorimeters [67], modulators (remote transmission) [68], thermal analyzers [69], energy converters [70], process and quality control. The demands for single element detectors for surveillance and environmental monitoring are growing rapidly.

Arrays used for thermal imaging are being applied to fire fighting, law enforcement (police, border patrol), mine detection, building monitoring, process control, driver's vision, pilot's vision enhancement (landing guidance), facial recognition, medical (surgery, trauma, chronic pain, open heart surgery, arthritis and rheumatism, vascular problems, neurological problems etc.), and traffic control.

References

1. J.F. Nye, *Physical properties of crystals* (Oxford University Press, London 1957).
2. M.E. Lines and A.M. Glass, *Principles and Applications of Ferroelectrics and Related Materials* (Oxford University Press, 1977).
3. S.B. Lang, *Ferroelectrics and Related Phenomenon*, edited by Lefkowitz and G. W. Taylor, **2**, Source book of Pyroelectricity (Gordon & Breach Science Publishers).
4. L.B. Schein, P.J. Cressman, and L.E. Cross, *Ferroelectrics*, **22**, 945 (1979).
5. Landolt-Börnstein, New Series, *Ferro- and Antiferroelectric Materials, Numerical Data and Functional Relationships in Science and Technology*, **III/3**, 1973, **III/5**, 1975; **III/11**, 1978; **III/18**, 1984; **III/29**, 1994; Eds., H. Hellwege and K.A. Hellwege (Springer-Verlag Publication).
6. A.G. Chynoweth, *Appl Phys*., **27**, 78 (1956); *Phys. Rev*., **117**, 1235 (1960).
7. R.L. Byer and C.B. Roundy, *Ferroelectrics*, **3**, 333 (1972).
8. R.W. Whatmore, *Reports on Progress in Physics*, **49**, 1335 (1986).
9. A.S. Bhalla, C.S. Fang, and L.E. Cross, *Appl. Physics Letters*, **43**, 932 (1983).
10. S.T. Liu, J.D. Zook, and D. Long, *Ferroelectrics*, **9**, 39 (1975).
11. A.S. Bhalla and L.E. Cross, *Ferroelectrics*, **38**, 935 (1981).
12. R.W. Whatmore, *Ferroelectrics*, **118**, 241–259 (1991).
13. *Eltec Catalog*, Eltec Instruments, Inc., (February 1995).
14. J.D. Rancourt, *Optical Thin Films User Handbook*, SPIE Optical Eng. Press, 1996, Bellingham, WA.
15. Optical Filters and Coatings, *Corion Catalog*, (1994).
16. *Handbook of Optics*, **1**, edited by M. Bass, Second Ed., (McGraw-Hill, Inc., New York, 1995).
17. J. Fraden, *Handbook of Modern Sensor* (AIP Press, Woodbury, New York, 1997).
18. S.G. Porter, *Ferroelectrics*, **33**, 193–206 (1981).
19. M.H. Lee et al., *SPIE*, **3061**, 170–178 (1997).
20. M.H. Lee and A. Bhalla, *J. Opt. Eng*., (in press).
21. S.B. Lang, *Ferroelectrics*, **34**, 71–94 (1981).
22. Y. Kuwano et al., *Ferroelectrics*, **46**, 175–183 (1983).
23. GEC-*Marconi Avionics*, Catalog, **1992**, (1992).
24. J.-S. Shie and P.K. Weng, *Sensors and Actuators A*, **33**, 183–189 (1992).
25. A. Handi and X. Gerbaux, *Infrared Phys*., **30**, 465–478 (1990).

26. G. Hass et al., *J. Opt. Soc. Am.*, **46**, 31–35 (1956).
27. A.D. Parson and D.J. Pedder, *J. Vac. Sci. Technol.*, **A6**, 1686–1689 (1988).
28. V.T. Bly and J.T. Cox, *Appl. Opt.*, *33*, 26–30 (1994).
29. K. Shibata et al., *Ferroelectrics*, **95**, 117–120 (1989).
30. K. Shibata et al., *Jpn. J. Appl. Phys.*, **26**, 1898–1902 (1987).
31. T. Yokoo et al., *Jpn. J. Appl. Phys.*, **26**, No. 7, 1082–1087 (1987).
32. R.W. Whatmore et al., *Ferroelectrics*, **104**, 269–283 (1990).
33. S.T. Liu et al., *Ferroelectrics*, **28**, 369–372 (1980).
34. A. van der Ziel and K.M. van Vliet, *Ferroelectrics*, ibid, **28**, 365–368 (1980).
35. N.M. Shorrocks et al., *SPIE*, **588**, 44–51 (1985).
36. M. Simhony et al., *IEEE, J. Quant. Mech.*, **QE-15**, 206–208 (1979).
37. R.M. Logan and K. Moore, *Infrared Phys.*, **13**, 37–47 (1973) and R.M. Logan, *Infrared Phys.*, **13**, 91–98 (1973).
38. E.H. Putley, *Infrared Phys.*, **21**, 173–179 (1981).
39. S.E. Stokowski, *Appl. Phys. Lett.*, **29**, 393–395 (1976).
40. E.H. Putley, *Infrared Phys.*, 18, 373–374 (1978).
41. N.E. Byer et al., *Appl. Phys. Lett.*, *27*, 639–641 (1975).
42. E.H. Putley, *Infrared Phys.*, **20**, 139–147 (1980).
43. J.Muggli and P. Waegli, *SPIE*, **395**, 225–232 (1983).
44. D.J. Pedder and S.G. Porter, *Allen Clark Res. Ctr. Ann. Rev.*, p. 41 (1984).
45. B.B. Lavrencic et al., *Ferroelectrics*, **91**, 323–328 (1989).
46. C. Hanson et al., *SPIE*, **1735**, 17–26 (1992).
47. R. Takayama et al., *Ferroelectrics*, **118**, 325–342 (1991).
48. M. Okuyama and Y. Hamakawa, *Ferroelectrics*, **118**, 261–278 (1991).
49. C. Ye et al., *Sensors and Actuators A*, **35**, 77–83 (1992).
50. M. Okuyama et al., *Ferroelectrics*, **91**, 127–139 (1989).
51. C.A. Cockrum, *SPIE*, **2685**, 2–15 (1996).
52. C.T. Elliott, *SPIE*, **2744**, 452–462 (1966).
53. M. Sano et al., *SPIE*, **2744**, 2–13 (1996).
54. R.J. Herring and P.E. Howard, *SPIE*, **2746**, 2–12 (1966).
55. R. Watton, *Ferroelectrics*, **91**, 87–108 (1989).
56. C.H. Lucas, *Sensors and Actuators A*, **25–27**, 147–154 (1991).
57. R. Watton and M.A. Todd, *Ferroelectrics*, **118**, 279–295 (1991).
58. D.A. Scribner et al., *Proc. IEEE*, **79**, 66–85 (1991).
59. GEC-Marconi, *Aerosense*, (April 21, 1997), Orlando, Fl.
60. R.S. Balcerak and T. DePersia, *SPIE*, **2685**, 74–79 (1996).
61. S. Middelhoek and A.C. Hoogerwerf, *Sensors and Actuators*, **10**, 1–8 (1986).
62. V.I. Vaganov, *Sensors and Actuators A*, **28**, 161–172 (1991).
63. S.T. Dunn, *Appl. Opt.*, **17**, 1367–1373 (1978).
64. M. Chirtoc and V. Tosa, *Ferroelectrics*, **118**, 307–311 (1991).
65. H. Niitsuma and R. Sato, *Ferroelectrics*, **34**, 37–45 (1981).
66. P. Ryser and S. Straessler, *Ferroelectrics*, **91**, 333–339 (1989).
67. S.B. Lang et al., *Ferroelectrics*, **73**, 431–447 (1987).
68. M.M. Pradhan et al., *Ferroelectrics*, **69**, 231–239 (1986).
69. H. Rahnamai, *Ferroelectrics*, **38**, 963–966 (1981).
70. R.B. Olsen et al., *Ferroelectrics*, **59**, 205–219 (1984).